

## A New Graphical Method to Diagnose the Impacts of Model Changes on Climate Sensitivity

**Shipra JAIN**

*Centre for Atmospheric Sciences, Indian Institute of Technology Delhi, India  
Department of Geophysics, Kyoto University, Kyoto, Japan  
School of Geosciences, University of Edinburgh, UK*

**Rattana CHHIN**

*Department of Geophysics, Kyoto University, Kyoto, Japan  
Research and Innovation Center, Institute of Technology of Cambodia, Cambodia*

**Ruth M. DOHERTY**

*School of Geosciences, University of Edinburgh, UK*

**Saroj K. MISHRA**

*Centre for Atmospheric Sciences, Indian Institute of Technology Delhi, India*

and

**Shigeo YODEN**

*Department of Geophysics, Kyoto University, Kyoto, Japan  
Institute for Liberal Arts and Sciences, Kyoto University, Kyoto, Japan*

*(Manuscript received 22 November 2019, in final form 15 December 2020)*

### Abstract

Equilibrium climate sensitivity (ECS) is defined as the change in the global mean surface air temperature due to the doubling or quadrupling of CO<sub>2</sub> in a climate model simulation. This metric is used to determine the uncertainty in future climate projections, and therefore, the impact of model changes on ECS is of large interest to the climate modeling community. In this paper, we propose a new graphical method, which is an extension of Gregory's linear regression method, to represent the impact of model changes on ECS, climate forcing, and climate feedbacks in a single diagram. Using this visualization method, one can (a) quantify whether the model or process change amplifies, reduces, or has no impact on global warming, (b) evaluate the percentage changes in ECS, climate forcing, and climate feedbacks, and (c) quantify the ranges of the uncertainties in the estimated changes. We demonstrate this method using an example of climate sensitivity simulations with and without interactive chemistry. This method can be useful for multimodel assessments where the response of multiple models for the same model experiment (e.g., usage of interactive chemistry compared with the prescribed chemistry as shown here) can be assessed simultaneously, which is otherwise difficult to compare and comprehend. We also

---

Corresponding author: Shigeo Yoden, Institute for Liberal Arts and Sciences, Kyoto University, Kyoto 606-8501, Japan  
E-mail: yoden.shigeo.53r@st.kyoto-u.ac.jp  
J-stage Advance Published Date: 13 January 2021



demonstrate how this method can be used to examine the spread in ECS, climate forcing, and climate feedbacks with respect to the multimodel mean (or one benchmark model) for multimodel frameworks such as Coupled Model Intercomparison Project Phase 5 or for different ensemble members in a large ensemble of simulations conducted using a single model.

**Keywords** new graphical method; climate sensitivity; interactive chemistry; climate forcing and climate feedbacks; multimodel assessments

**Citation** Jain, S., R. Chhin, R. M. Doherty, S. K. Mishra, and S. Yoden, 2021: A new graphical method to diagnose the impacts of model changes on climate sensitivity. *J. Meteor. Soc. Japan*, **99**, 437–448, doi:10.2151/jmsj.2021-021.

## 1. Introduction

The Earth's climate is sensitive to the concentrations of greenhouse gases (GHGs) in the atmosphere. The concentrations of GHGs have a large impact on radiative forcing and surface climate change. One widely used metric to estimate this impact is equilibrium climate sensitivity (ECS). ECS, which is defined as the response of global and annual mean surface air temperatures to a change in GHG concentrations, can be calculated using an idealized long-period climate simulation in which atmospheric CO<sub>2</sub> concentration is instantaneously doubled ( $2 \times \text{CO}_2$ ) or quadrupled ( $4 \times \text{CO}_2$ ) from the pre-industrial (PI) level. Climate sensitivity is also used as a measure of uncertainty for the assessment of future projections in similarly forced general circulation models (GCMs) or Earth system models (ESMs). A wide range of climate sensitivity across models would imply a lower confidence in future projections, and thus, continuous efforts are being made to determine and understand the factors on which the climate sensitivity depends in models.

Recent research shows that using interactive chemistry instead of prescribed values, as done in Coupled Model Intercomparison Project Phase 5 (CMIP5), can impact surface climate and estimates of ECS in climate models (e.g., Chiodo et al. 2016; Dietmüller et al. 2014; Marsh et al. 2016; Muthers et al. 2014; Nowack et al. 2015, 2017, 2018). Nowack et al. (2015), using the UK Met Office chemistry-climate model, showed that the global mean surface warming is reduced by  $\sim 1$  K ( $\sim 20\%$ ) when the model computes the chemistry processes interactively instead of using prescribed values at PI levels. In contrast to this, Marsh et al. (2016) showed no large impacts of interactive chemistry on the climate sensitivity in the Community Earth System Model–Whole Atmosphere Community Climate Model.

To evaluate the response of surface climate to the

imposed forcing (doubling or quadrupling of CO<sub>2</sub>), these studies used the following linear energy balance equation introduced by Gregory et al. (2004) and used by others (Aldrin et al. 2012; Andrew et al. 2012; Annan and Hargreaves 2006; Dessler and Forster 2018; Lewis and Curry 2015; Otto et al. 2013; Skeie et al. 2014):

$$N(t) = F + \alpha \Delta T(t), \quad (1)$$

where  $t$  is time (annual mean),  $N(t)$  is the net radiative flux ( $\text{W m}^{-2}$ ) at the top of the atmosphere (TOA),  $F$  is the imposed forcing ( $\text{W m}^{-2}$ ),  $\alpha$  is the climate feedback parameter ( $\text{W m}^{-2} \text{K}^{-1}$ ), and  $\Delta T(t)$  is the global mean surface air temperature change (K). Equation (1) is linear, and therefore,  $F$  can be estimated by the  $y$ -axis intercept and  $\alpha$  by the slope of the line of best fit from the scatter plot of  $\Delta T(t)$  versus  $N(t)$ . ECS is defined as the global mean surface air temperature change  $\Delta T$  in response to abrupt  $2 \times \text{CO}_2$  or  $4 \times \text{CO}_2$  experiments (Andrews et al. 2012) under the limit of time  $t$  tending to very large values (generally hundreds of years for atmosphere–ocean coupled GCMs). It is a convenient metric for quantifying the joint effect of climate forcing and climate feedbacks under the implicit assumption of  $N$  approaching zero. ECS is given as  $-F/\alpha$  in a  $2 \times \text{CO}_2$  experiment, whereas it is  $-F/(2\alpha)$  in a  $4 \times \text{CO}_2$  experiment.

Although the information that is provided in the climate sensitivity studies is of extreme importance for future climate change assessments, the results presented in these papers can be challenging to comprehend unless accompanied by a detailed textual description. These studies also emphasize the need for multimodel assessments in which each model's response to the interactive chemistry should be compared with its prescribed chemistry simulation and also with the results of other models for the same experiment. However, in that case, the intercomparison of the myriad of results will be complex. To overcome this, we propose

a new graphical method in which information that is typically presented in the form of text and tables can be summarized and collated in one single diagram.

One of the applications of this method is for multi-model assessments in which the impact of model or process change on ECS, climate forcing, and climate feedbacks can be simultaneously diagnosed for multiple models. Using the proposed method, each model can be represented by its own marker with standard error intervals in a single diagram, which simplifies the intercomparison of multiple models for the same experimental framework (e.g., using interactive chemistry instead of prescribed values in each model). In this paper, we demonstrate this method using the example of climate sensitivity simulations with interactive and prescribed chemistry, conducted using Japan Meteorological Agency–Meteorological Research Institute (JMA-MRI) Earth System and coupled atmosphere-ocean models. We also show how this method can be used to estimate the spread in ECS, climate forcing, and climate feedbacks for multiple models with respect to the multimodel mean (MMM) or a benchmark model, using CMIP5/6 or other data. This method can also be used to estimate the spread or change in these three parameters for a large ensemble of simulations done by using a single model.

Section 2 describes the method and data that are used in this paper. Section 3 demonstrates the application of this graphical method for three different examples, and Section 4 summarizes the key highlights of this paper.

## 2. Description of the method and data

### 2.1 Linear regression to estimate forcing and feedbacks

We first present a general form of this method for two sets of climate sensitivity simulations with (i) a control (ctrl) simulation and (ii) an experiment (expt) simulation, which is the same as ctrl but with a model process or a parameter value changed to investigate its impact on climate sensitivity.

For a simulation  $x$  ( $=$  ctrl or expt), the change in global mean surface air temperature in the abrupt  $4 \times \text{CO}_2$  experiment (denoted by 4C in subscript) with respect to the PI climatology is given as

$$\Delta T_x(t) = T_{4C,x}(t) - \bar{T}_{PI,x}, \quad (2)$$

where  $T_{4C,x}(t)$  is the global mean surface air temperature (K) in the 4C experiment and  $\bar{T}_{PI,x}$  is the climatological (time mean) temperature for the PI simulation. Similarly, a change in the net radiation flux is given as

$$\Delta N_x(t) = N_{4C,x}(t) - \bar{N}_{PI,x}. \quad (3)$$

Note that Eq. (1) is for the scenario where the model is initially in an equilibrium state such that the net radiative imbalance at the TOA is zero in the PI simulation. However, if the model is in an initial non-stationary state (i.e., the value of  $N$  in the PI simulation is non-zero), one should remove the radiative imbalance noted in the PI simulation from the 4C simulation. In this case, the variable  $N$  should be replaced by  $\Delta N$  to account for the radiative imbalance, if there is any, in the initial state. Equation (1) can, therefore, be re-written as

$$\Delta N_x(t) = F_x + \alpha_x \Delta T_x(t), \quad (4)$$

where  $\Delta N_x(t)$  and  $\Delta T_x(t)$  can be regressed for ctrl and expt simulations separately for the full simulation period after the abrupt quadrupling of the  $\text{CO}_2$ , and the values for the climate feedback parameter  $\alpha_x$  ( $x =$  ctrl or expt) and the imposed forcing  $F_x$  are estimated using the lines of best fit.

### 2.2 Impact analysis

As Eq. (4) can be re-written as  $\Delta T_x(t) = (\Delta N_x(t) - F_x)/\alpha_x$ , the ratio of the two  $\Delta T_x(t)$  for ctrl and expt is given by

$$\frac{\Delta T_{\text{expt}}(t)}{\Delta T_{\text{ctrl}}(t)} = \frac{\alpha_{\text{ctrl}}}{\alpha_{\text{expt}}} \times \frac{\Delta N_{\text{expt}}(t) - F_{\text{expt}}}{\Delta N_{\text{ctrl}}(t) - F_{\text{ctrl}}} = \frac{R_F(t)}{R_\alpha}, \quad (5)$$

where  $R_\alpha$  is the ratio of the climate feedback parameter  $\alpha_x$  for ctrl and expt and  $R_F(t)$  is the ratio of the difference between the net radiation flux at the TOA and the imposed forcing,  $\Delta N_x(t) - F_x$ , for ctrl and expt. From this relationship, the impact of expt on the global mean surface air temperature change in the ctrl simulation is given by

$$\Delta T_{\text{expt}}(t) - \Delta T_{\text{ctrl}}(t) = \left( \frac{R_F(t)}{R_\alpha} - 1 \right) \times \Delta T_{\text{ctrl}}(t). \quad (6)$$

Note that Eq. (6) can be used to determine the time evolution of the change in the global mean surface air temperature. To determine the equilibrium response of the surface air temperature, i.e., ECS, we replace all time-varying components in Eq. (6) with their respective climatological means:

$$\overline{\Delta T_{\text{expt}}} - \overline{\Delta T_{\text{ctrl}}} = \left( \frac{\overline{R_F}}{R_\alpha} - 1 \right) \times \overline{\Delta T_{\text{ctrl}}}, \quad (7)$$

where  $\overline{R_F} = (\overline{\Delta N_{\text{expt}}} - F_{\text{expt}})/(\overline{\Delta N_{\text{ctrl}}} - F_{\text{ctrl}})$ , and  $\overline{\Delta N_x}$  must be calculated for the period when the model is in equilibrium or quasi-equilibrium state, excluding

the initial transient response to the abrupt quadrupling of CO<sub>2</sub>. Note that the % change in ECS in the expt simulation with respect to ctrl simulation is given as  $[(\bar{R}_F/R_\alpha) - 1] \times 100$ .

Equation (7) leads to five possible scenarios (Cases 0 to IV) as follows:

Case 0:  $\bar{R}_F = R_\alpha$  and  $\Delta T_{ctrl} = \text{any value}$ ,

represents the case that the impact of the experiment on the global mean surface air temperature, i.e., ECS, is zero.

Case I:  $\bar{R}_F > R_\alpha$  and  $\Delta T_{ctrl} > 0$ ,

represents the case of global warming as  $\Delta T_{ctrl} > 0$ , and the warming is amplified.

Case II:  $\bar{R}_F > R_\alpha$  and  $\Delta T_{ctrl} < 0$ ,

represents the case of global cooling as  $\Delta T_{ctrl} < 0$ , and the cooling is amplified.

Case III:  $\bar{R}_F < R_\alpha$  and  $\Delta T_{ctrl} > 0$ ,

represents the case of global warming as  $\Delta T_{ctrl} > 0$ , and the warming is reduced.

Case IV:  $\bar{R}_F < R_\alpha$  and  $\Delta T_{ctrl} < 0$ ,

represents the case of global cooling as  $\Delta T_{ctrl} < 0$ , and the cooling is reduced.

### 2.3 Uncertainty in feedback parameter, forcing, and their ratios

Given that the relationship between  $\Delta N_x(t)$  and  $\Delta T_x(t)$  is not entirely linear in a model simulation, there will be associated uncertainties in  $\alpha_x$  and  $F_x$  that are estimated using linear regression. The possible values for  $\alpha_x$  are given by  $\alpha_x \pm E_{\alpha,x}$  and  $F_x$  by  $F_x \pm E_{F,x}$ , where  $E_{\alpha,x}$  and  $E_{F,x}$  are the uncertainties in  $\alpha_x$  and  $F_x$ , respectively. The uncertainties (or the standard errors),  $E_\alpha$  and  $E_F$ , are given as follows (e.g., Montgomery et al. 2012):

$$E_{\alpha,x}^2 = \frac{\sigma_x^2 I}{I \sum_{i=1}^I (\Delta T_{x,i})^2 - \left( \sum_{i=1}^I \Delta T_{x,i} \right)^2}, \quad (8)$$

$$E_{F,x}^2 = \frac{\sigma_x^2 \sum_{i=1}^I (\Delta T_{x,i})^2}{I \sum_{i=1}^I (\Delta T_{x,i})^2 - \left( \sum_{i=1}^I \Delta T_{x,i} \right)^2}, \quad (9)$$

where  $i$  is a sequential integer for each year and  $I$  is the total number of years used for the linear regression, and  $\sigma_x$  is given as

$$\sigma_x^2 = \frac{\sum_{i=1}^I (\Delta N_{x,i} - F_x - \alpha_x \Delta T_{x,i})^2}{I - 2}. \quad (10)$$

The uncertainties  $E_{\alpha,x}$  and  $E_{F,x}$  are obtained for both ctrl and expt simulations. The magnitudes of uncertainty for the ratios  $R_\alpha$  and  $R_F$  are also obtained using

the law of propagation of errors (e.g., Bohm and Zech 2014):

$$E_{R_\alpha} = R_\alpha \sqrt{\left( \frac{E_{\alpha,x,expt}}{\alpha_{expt}} \right)^2 + \left( \frac{E_{\alpha,x,ctrl}}{\alpha_{ctrl}} \right)^2}, \quad (11)$$

$$E_{R_F} = R_F \sqrt{\left( \frac{E_{H,x,expt}}{H_{expt}} \right)^2 + \left( \frac{E_{H,x,ctrl}}{H_{ctrl}} \right)^2}, \quad (12)$$

$$H_x = \overline{\Delta N}_x - F_x, \quad (13)$$

$$E_{H,x} = \sqrt{E_{\overline{\Delta N}_x}^2 + E_{F,x}^2}, \quad (14)$$

where  $E_{\overline{\Delta N}_x}$  is the standard error in  $\overline{\Delta N}_x$  and given as:

$$E_{\overline{\Delta N}_x} = \frac{\sigma_{\Delta N,x}}{\sqrt{J}}, \quad (15)$$

where  $J$  is the number of model years used to calculate  $\overline{\Delta N}_x$  and  $\sigma_{\Delta N,x}$  is the standard deviation in  $\Delta N_x(t)$  for the  $J$  years.

It is also noted that each year in  $\Delta T(t)$  and  $\Delta N(t)$  time series is not independent (Gregory et al. 2004), which would lead to the underestimation of the errors calculated above. The appropriate statistical confidence intervals can be obtained by replacing the total number of model years used for the error estimation (i.e.,  $I$  or  $J$ ) with the effective number of years estimated after the consideration of time lag correlation (e.g., Naito and Yoden 2005) or by using the bootstrapping method as used by Andrews et al. (2012).

### 2.4 Model simulations and data

We demonstrate the application of this method using two sets of simulations, namely, (i) PI and 4C simulations with prescribed chemistry (FIXED, instead of ctrl above) and (ii) PI and 4C simulations with interactive chemistry (ACTIVE, instead of expt above). For the experiments with the prescribed chemistry (PI FIXED and 4C FIXED), the MRI atmosphere-ocean-aerosol GCM, CGCM3 (Yukimoto et al. 2012) was used. The simulations with interactive chemistry (PI ACTIVE and 4C ACTIVE) were conducted using MRI ESM1 (Earth System Model version 1, Adachi et al. 2013; Yukimoto et al. 2011).

The MRI ESM1 and CGCM3 models applied in this study are the same as those used by Noda et al. (2017, 2018) for similar PI FIXED and PI ACTIVE experiments for paleoclimates (Mid-Holocene and the Last Glacial Maximum, respectively). Although the MRI-ESM1 simulations in CMIP5 applied the carbon cycle processes, the carbon cycle processes were deactivated in the ESM1 simulations conducted here

(for both PI and 4C). Both MRI ESM1 and CGCM3 have the same components except for the chemical component, which includes 90 chemical species with 172 gas-phase reactions, 59 photolysis reactions, and 16 heterogeneous reactions and also includes improved grid-scale transport with a semi-Lagrangian scheme (Yukimoto et al. 2011). For the FIXED PI and 4C simulations, the concentrations of the chemical species are prescribed at 1850 level. The stratosphere includes seasonal and latitude–height variations of the chemical species, whereas the troposphere includes seasonal and 3-D variations of the species. The ozone values are taken from the Atmospheric Chemistry and Climate/Stratosphere-troposphere Processes and their Role in Climate (ACC/SPARC) database (<https://climatedataguide.ucar.edu/climate-data/stratospheric-tropospheric-ozone-accsparc-atmospheric-chemistry-and-climate>). The concentrations of other GHGs and anthropogenic aerosols or their precursors at 1850 level are taken from the Representative Concentration Pathways (RCP) database (<http://www.iiasa.ac.at/web-apps/tnt/RcpDb>). More details on the prescribed chemical species are provided in Yukimoto et al. (2012). For ACTIVE PI and 4C simulations, the model had the initial chemical concentrations at 1850 level, which were taken from the “esmControl” run in CMIP5, which is the same as the ACTIVE PI simulation here.

For PI simulations, we use the same datasets of 100 years as obtained by Noda et al. (2017) for both FIXED and ACTIVE simulations. There is no significant climate drift noted in the 100 year PI simulation. For 4C simulations (both FIXED and ACTIVE), the model was started using the restart files of the corresponding PI runs and run for 110 years in total, with the CO<sub>2</sub> quadrupled abruptly after 10 years. The horizontal resolution of the model was a triangular truncation at the maximum wavenumber 42 (T42), corresponding to a grid resolution of ~2.8° across longitude and latitude. The model had 68 vertical layers (L68) extending from the surface to the mesopause, 0.01 hPa (Deushi and Shibata 2011). The treatment of water vapor feedback was similar to that described in Noda et al. (2018). More details on the model setup can be found in Noda et al. (2017, 2018).

The output data from 16 CMIP5 models were also used to demonstrate the application of this method for multimodel frameworks (Subsection 3.3). The CMIP5 data were obtained from the Earth System Grid Federation (ESGF) website (<https://esgf-node.llnl.gov/search/esgf-llnl/>).

### 3. Results

#### 3.1 Demonstration of the method—Impact of interactive chemistry

To demonstrate this graphical method, we use the two sets of climate sensitivity simulation data generated from the MRI models, i.e., ACTIVE and FIXED for PI and 4C simulations as described in the previous section. Figure 1a shows the time series of  $\Delta T_x(t)$  as given by Eq. (2) for ACTIVE (blue) and FIXED (red) simulations. The vertical dotted line marks the time  $t = 0$  when CO<sub>2</sub> concentration is quadrupled and the time before  $t = 0$  corresponds to the PI condition. The response of the global mean surface air temperature anomalies to the abrupt  $4 \times$  CO<sub>2</sub> is evident in the initial few decades, and the temperature changes asymptote to a similar value for both ACTIVE and FIXED simulations for around the last 50 years.

Figure 1b shows  $\Delta N_x(t)$  versus  $\Delta T_x(t)$  for the last 100 years of ACTIVE and FIXED simulations. The initial 10 years of the 110 year simulation are discarded as they correspond to the period before the quadrupling of CO<sub>2</sub> concentration. Figure 1b confirms the almost linear relationship between  $\Delta N_x(t)$  and  $\Delta T_x(t)$ , and  $\alpha_x$  and  $F_x$  are estimated by the slope and intercept of the lines of best fit (solid blue and red lines, respectively). Note that we use the data for the full  $4 \times$  CO<sub>2</sub> period (i.e., 100 years) to determine the coefficients  $\alpha_x$  and  $F_x$  using linear regression. The ratio  $R_\alpha$  is obtained using  $\alpha_x$ , and the ratio  $\bar{R}_F$  is obtained from  $\overline{\Delta N_x}$  and  $F_x$  as defined in Eq. (7). To calculate the climatological mean of  $\Delta N_x$ , i.e.,  $\overline{\Delta N_x}$ , we use data for the last 50 years of the simulation period, when the model is in a quasi-equilibrium state. The values of  $\overline{\Delta N_x}$  are shown by horizontal dotted lines with the corresponding color in Fig. 1b. The standard errors in  $\alpha_x$  are estimated using Eqs. (8) and (10), and those in  $F_x$  are estimated using Eqs. (9) and (10), with  $i = 1$  to 100 ( $= J$ ). The errors in  $\overline{\Delta N_x}$  are calculated using Eq. (15), with  $J = 50$ . The errors in  $R_\alpha$  and  $\bar{R}_F$  are estimated using Eqs. (11)–(15). Table 1 provides the values of all quantities and their corresponding errors.

Figure 2 shows the obtained value of  $R_\alpha$  and  $\bar{R}_F$  (black dot) with its standard errors (horizontal and vertical bars, as described in Subsection 2.3) on  $R_\alpha - \bar{R}_F$  plane. Figure 2 is our proposed new graphic method to visualize the impact of model changes on ECS, climate forcing, and climate feedbacks. The abscissa,  $R_\alpha$ , represents the ratio of the climate feedback parameter. The unity value of  $R_\alpha$  represents no change in the climate feedback parameter  $\alpha_x$ , and every 0.1 increase (or decrease) in the magnitude of

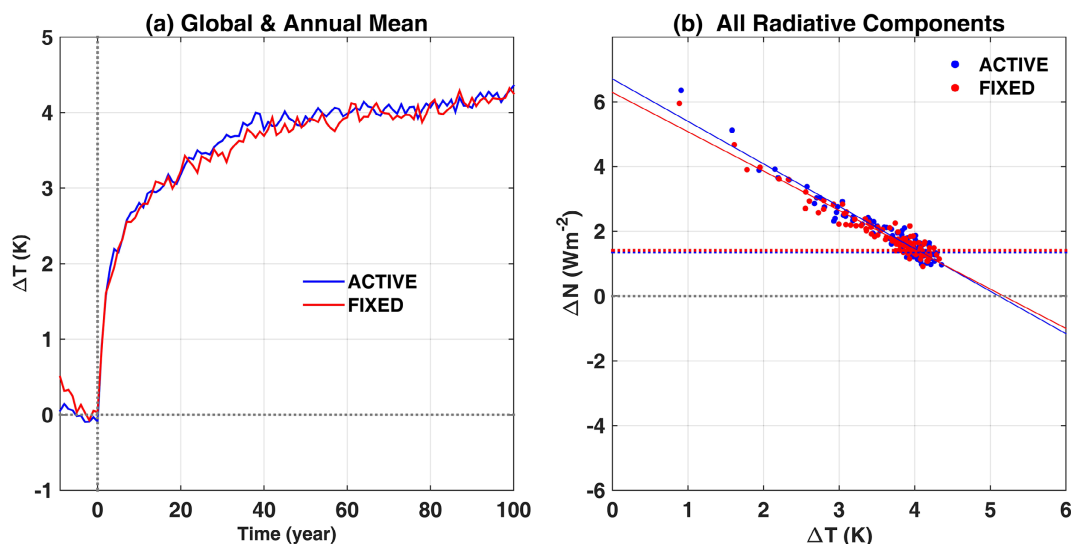


Fig. 1. (a) Time series of global and annual mean surface air temperature anomaly,  $\Delta T_x(t)$ , for ACTIVE (blue) and FIXED (red) simulations. (b) Net radiative flux (all components) at the TOA,  $\Delta N_x(t)$ , versus  $\Delta T_x(t)$  for each year for ACTIVE (blue dots) and FIXED (red dots) simulations. Corresponding lines represent ordinary least squares regression fits to the last 100 year data. Dotted lines parallel to abscissa correspond to the time mean of  $\Delta N_x(t)$  for the last 50 years.

Table 1. Summary of the parameters obtained from the linear regression fits and uncertainty in their estimation.

	All radiation	CS LW	CS SW	CRE LW	CRE SW
$\alpha_{ACTIVE} \pm E_{\alpha, ACTIVE}$	$-1.312 \pm 0.037$	$-2.048 \pm 0.016$	$0.819 \pm 0.014$	$-0.175 \pm 0.019$	$0.093 \pm 0.029$
$\alpha_{FIXED} \pm E_{\alpha, FIXED}$	$-1.215 \pm 0.035$	$-2.000 \pm 0.014$	$0.850 \pm 0.014$	$-0.218 \pm 0.021$	$0.154 \pm 0.029$
$F_{ACTIVE} \pm E_{F, ACTIVE}$	$6.708 \pm 0.137$	$7.561 \pm 0.060$	$0.309 \pm 0.054$	$-1.256 \pm 0.073$	$0.094 \pm 0.108$
$F_{FIXED} \pm E_{F, FIXED}$	$6.290 \pm 0.129$	$7.714 \pm 0.052$	$0.094 \pm 0.052$	$-1.345 \pm 0.076$	$-0.173 \pm 0.105$
$\overline{\Delta N}_{ACTIVE} \pm E_{N, ACTIVE}$	$1.363 \pm 0.031$	$-0.813 \pm 0.034$	$3.645 \pm 0.016$	$-1.975 \pm 0.017$	$0.506 \pm 0.024$
$\overline{\Delta N}_{FIXED} \pm E_{N, FIXED}$	$1.413 \pm 0.032$	$-0.352 \pm 0.038$	$3.519 \pm 0.018$	$-2.208 \pm 0.018$	$0.454 \pm 0.027$
$R_{\alpha} \pm E_{R_{\alpha}}$	$1.080 \pm 0.043$	$1.024 \pm 0.011$	$0.964 \pm 0.023$	$0.803 \pm 0.117$	$0.600 \pm 0.219$
$R_F \pm E_{R_F}$	$1.096 \pm 0.041$	$1.038 \pm 0.012$	$0.974 \pm 0.023$	$0.833 \pm 0.115$	$0.657 \pm 0.210$
% change in ECS $\pm \delta ECS$ (%)	$1.502 \pm 5.597$	$1.391 \pm 1.574$	$1.015 \pm 3.381$	$3.737 \pm 20.806$	$9.404 \pm 53.048$

$R_{\alpha}$  corresponds to the 10% increase (or decrease) in feedback strength in ACTIVE simulation compared with FIXED simulation. Similarly, the unity value on the ordinate,  $\bar{R}_F = 1$ , represents no change in the difference between radiative flux imbalance and forcing ( $\overline{\Delta N}_x - F_x$ ).

The % change in ECS in ACTIVE simulation with respect to that in FIXED simulation is given by  $[(\bar{R}_F/R_{\alpha}) - 1] \times 100$ . The thick black dashed line represents Case 0 as described in Subsection 2.2 with  $\bar{R}_F = R_{\alpha}$  and therefore corresponds to the case of no impact of the experiment on the global mean surface air temperature or ECS. This line is referred to as the no-impact line. Any point lying above this no-impact

line corresponds to Case I (as  $\Delta T_{ctrl} > 0$ ) with  $\bar{R}_F > R_{\alpha}$ , and thus represents the amplification of global warming in the ACTIVE compared with the FIXED simulation. On the other hand, any point lying below the no-impact line corresponds to Case III with  $\bar{R}_F < R_{\alpha}$ , representing the reduction of global warming in ACTIVE simulation compared with that in FIXED simulation. Four red (blue) dashed lines in the plot show consecutive 10% increases (decreases) in the values of ECS of up to  $\pm 40\%$ :  $\bar{R}_F = \left(1 \pm \frac{a\%}{100\%}\right) R_{\alpha}$ , ( $a = 10, 20, 30, \text{ and } 40$ ).

In the present example,  $R_{\alpha}$  is  $\sim 1.08 \pm 0.04$ , which implies that the climate feedback parameter  $\alpha_x$  is

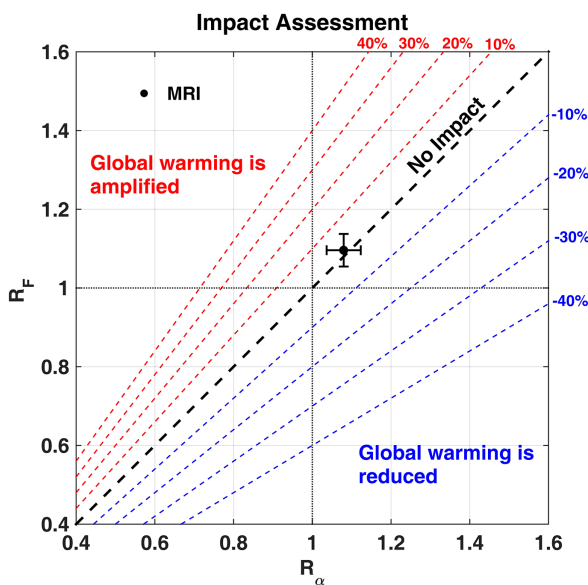


Fig. 2. Graphical representation of the impact of ACTIVE simulation compared with FIXED one on ECS, climate forcing, and climate feedbacks for MRI models, as denoted by a black dot. The abscissa  $R_\alpha$  shows the ratio of the feedback parameter, whereas the ordinate  $R_F$  shows the ratio of the difference between the net radiation flux at the TOA and the imposed forcing. The red and blue dashed lines correspond to the % changes in ECS. Thick black dashed line shows the no-impact line and represents no impact on global warming ( $R_F = R_\alpha$ ; Case 0). The region above the no-impact line corresponds to amplification of global climate change ( $R_F > R_\alpha$ ; Case I for global warming or Case II for global cooling), whereas the region below the no-impact line corresponds to a reduction of global climate change ( $R_F < R_\alpha$ ; Case III for global warming or Case IV for global cooling). Solid black error bars show the uncertainties in  $R_\alpha$  and  $R_F$ . The unity value of  $R_\alpha$  represents no change in the climate feedback parameter  $\alpha_x$ , and every 0.1 increase (or decrease) in the magnitude of  $R_\alpha$  corresponds to the 10 % increase (or decrease) in feedback strength in ACTIVE simulation compared with that in FIXED simulation. Similarly, the unity value of  $R_F$  represents no change, and every  $\pm 0.1$  increase in  $R_F$  represents a  $\pm 10$  % change in the difference of radiative flux imbalance and forcing.

increased by  $\sim 8$  % in ACTIVE simulation compared with FIXED simulation with the standard error of  $\pm 4$  %. Similarly,  $\bar{R}_F$  is  $\sim 1.10 \pm 0.04$ , which means the difference between radiative flux imbalance and

forcing ( $\overline{\Delta N_x} - F_x$ ) is also increased by  $\sim 10$  % with a standard error of 4 %. Consequently, the ratio  $\bar{R}_F/R_\alpha$  remains close to 1 with only a 1.5 % increase in ECS. It can be concluded from Fig. 2 that the impact of interactive chemistry on ECS is small in the MRI climate models. The scatter in the linear fit for  $\Delta N_x(t)$  versus  $\Delta T_x(t)$  is quite small for the MRI models (Fig. 1b), and thus, the uncertainties are also small. We have data only from MRI models for this demonstration, and hence, there is only one symbol in Fig. 2. However, if the multimodel outputs are available for the same experimental framework (e.g., for interactive and prescribed chemistry), then each model can be plotted by its own symbol in this diagram, and the intercomparison of ECS, climate forcing, and climate feedbacks for the multiple models is straightforward.

### 3.2 Application to individual radiative components

According to the linear climate feedback theory, the net global climate feedback is the linear sum of longwave (LW) and shortwave (SW) contributions for each clear sky (CS) and cloud radiative effect (CRE) component, as described in the Methods section of Nowack et al. (2015). The net radiative imbalance at the TOA due to all-radiative components is the linear sum of the imbalance caused by the four individual components (CS-LW, CS-SW, CRE-LW, and CRE-SW).

The corresponding values of  $\Delta N(t)$  and  $\Delta T(t)$  are almost linearly related to the individual radiative components in each FIXED and ACTIVE simulation as shown in Figs. 3a and 3b. The values of all metrics for the individual radiative components are obtained by estimating Gregory’s linear relations for CS and CRE components separately and given in Table 1. The CS radiative feedback, which is given by the slope of the line of best fit, is much larger in magnitude than the CRE feedback for both LW and SW components. Furthermore, the feedback for LW and SW components is opposite in sign with larger magnitudes for LW for both the CS and CRE components (see Table 1 for the estimated values). This indicates that the LW feedbacks in the atmosphere are partially offset by the corresponding SW feedbacks.

The values of  $R_\alpha$  and  $\bar{R}_F$  (and their uncertainties) for individual and all-radiative components are plotted in Fig. 3c. The CRE-SW (CRE-LW) component shows a large reduction of  $\sim 40.0$  % ( $\sim 19.7$  %) in the climate feedback with a relatively smaller reduction of  $\sim 34.3$  % ( $\sim 16.7$  %) in the climate forcing, thus indicating a net amplification of the global warming by  $\sim 9.4$  % ( $\sim 3.7$  %) in ACTIVE simulation com-

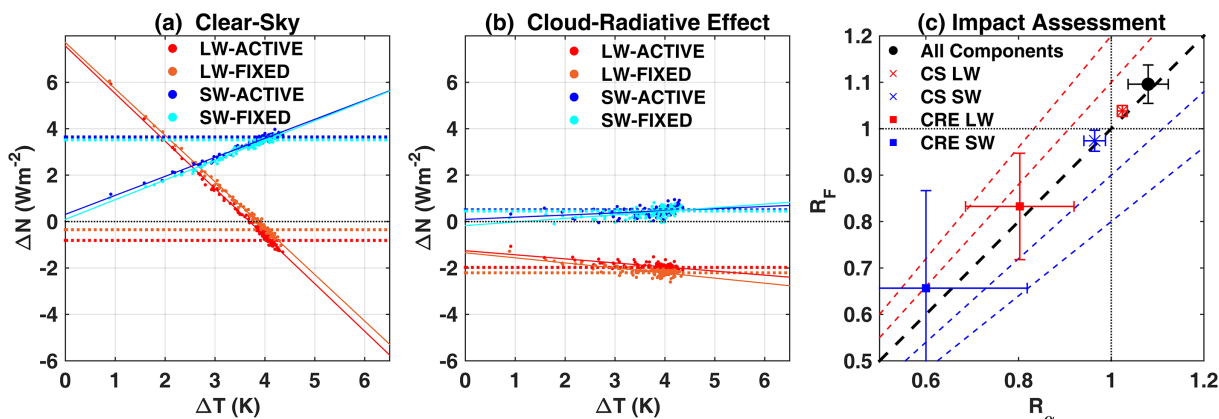


Fig. 3. (a) The same as in Fig. 1b but for clear sky (CS) longwave (LW) and shortwave (SW) components for ACTIVE and FIXED simulations for 100 years. (b) The same as in (a) but for cloud radiative effect (CRE). (c) Impact assessment on  $R_\alpha$ – $R_F$  plane for individual and all-radiative components.

pared with that in FIXED simulation. Both CS-LW and CS-SW components show small changes with the same tendency in the feedback and forcing ( $\sim 2$ – $4$  % increase and  $\sim 3$ – $4$  % decrease, respectively); thus, the ratios  $R_\alpha$  and  $\bar{R}_F$  for these components remain close to one. The uncertainties in ratios  $R_\alpha$  and  $\bar{R}_F$  are also larger for CRE components than for CS components, which is also confirmed by Figs. 3a and 3b, showing larger scatter in CRE components than in CS components.

ACTIVE simulation leads to slight amplification of global warming by  $\sim 1.5$  % compared with FIXED simulation for all-radiative components (black circle), as described in Subsection 3.1. The individual radiative components, CS-LW and CS-SW components lie near the no-impact line and show slight amplification of global warming by approximately 1 %. The CRE-LW and CRE-SW components show amplification of global warming by approximately 4 % and 9 %, respectively (the bottom row in Table 1). Also, notably, each radiation component is regressed against the same  $\Delta T$ , and ideally, the impact of individual components on temperatures should be the same and close to the impact noted for the all-radiative component. Here, however,  $R_\alpha$  and  $\bar{R}_F$  for CRE have a large impact and uncertainty compared with the all-radiative component. The large uncertainties in the CRE component arise because of the large scatter in the linear fit and smaller values of climate feedback and climate forcing than those in the CS component as shown in Figs. 3a and 3b (see also Eqs. 11 and 12).

### 3.3 Application to multiple CMIP5 models

In the previous subsections, we showed the impact of interactive chemistry on ECS, climate forcing, and climate feedbacks for the JMA-MRI climate models as shown in Figs. 2 and 3c. To compare the outputs of multiple models, the results for other models with the same experimental framework can also be included in this diagram. Note that in this case, the impact of chemistry is examined by comparing ACTIVE (expt) simulation for each model with respect to its own FIXED (ctrl) simulation.

Here, we demonstrate to use of this method to visualize the spread in ECS, climate forcing, and climate feedbacks across multiple CMIP5 models. In this case, ctrl simulation can be replaced with the MMM, and each model can be used as an expt simulation, to examine the relative difference of ECS, climate forcing, and climate feedbacks for each model from those for the MMM. Figure 4 shows the relative difference of 18 models (16 CMIP5 models and two MRI models used above) from the MMM ( $\bar{R}_F = R_\alpha = 1$ ), plotted with their own symbols as listed.

The CMIP5 models show a large spread in ECS varying from approximately  $-38$  % to  $35$  % with respect to the MMM (see Table 2 for the parameter values and standard errors of each model). In total, 10 models show more global warming when compared with the MMM (above the black dashed line), whereas the rest of the models show less global warming (below the black dashed line) when compared with the MMM. The climate forcing shows a large spread from approximately  $-43$  % to  $39$  % when compared with the MMM (see  $\bar{R}_F$  of the sixth column in Table 2).

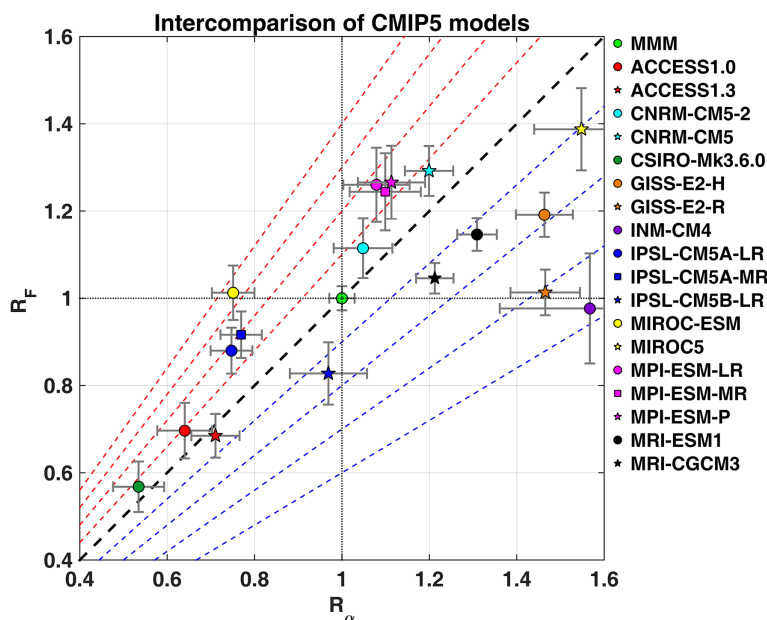


Fig. 4. Intercomparison of CMIP5 models for abrupt  $4 \times \text{CO}_2$  experiment relative to the multimodel mean (MMM;  $R_F = R_\alpha = 1$ ). Each model is plotted with its own symbol with standard errors in  $R_F - R_\alpha$  plane. See the main text for details.

Table 2. Summary of parameters obtained for CMIP5 models for abrupt  $4 \times \text{CO}_2$  experiment.

	$\alpha \pm E_\alpha$	$F \pm E_F$	$\overline{\Delta N} \pm E_N$	$R_\alpha \pm E_{R_\alpha}$	$R_F \pm E_{R_F}$	% change in ECS $\pm \delta\text{ECS}$ (%)
MMM	$-1.002 \pm 0.020$	$6.542 \pm 0.090$	$1.878 \pm 0.017$	$1.000 \pm 0.029$	$1.000 \pm 0.028$	–
ACCESS1.0	$-0.641 \pm 0.062$	$5.273 \pm 0.287$	$2.024 \pm 0.043$	$0.640 \pm 0.063$	$0.697 \pm 0.064$	$8.811 \pm 14.602$
ACCESS1.3	$-0.712 \pm 0.053$	$5.259 \pm 0.223$	$2.066 \pm 0.032$	$0.711 \pm 0.055$	$0.685 \pm 0.050$	$-3.621 \pm 10.291$
CNRM-CM5-2	$-1.050 \pm 0.064$	$7.260 \pm 0.301$	$2.062 \pm 0.029$	$1.048 \pm 0.067$	$1.115 \pm 0.068$	$6.345 \pm 9.436$
CNRM-CM5	$-1.202 \pm 0.050$	$7.738 \pm 0.238$	$1.713 \pm 0.030$	$1.199 \pm 0.055$	$1.292 \pm 0.057$	$7.723 \pm 6.893$
CSIRO-Mk3.6.0	$-0.536 \pm 0.057$	$4.638 \pm 0.259$	$1.990 \pm 0.054$	$0.535 \pm 0.058$	$0.568 \pm 0.058$	$6.231 \pm 15.860$
GISS-E2-H	$-1.466 \pm 0.058$	$7.115 \pm 0.208$	$1.559 \pm 0.028$	$1.463 \pm 0.065$	$1.191 \pm 0.051$	$-18.580 \pm 5.017$
GISS-E2-R	$-1.468 \pm 0.074$	$6.518 \pm 0.224$	$1.792 \pm 0.027$	$1.465 \pm 0.080$	$1.013 \pm 0.052$	$-30.841 \pm 5.179$
INM-CM4	$-1.570 \pm 0.204$	$6.292 \pm 0.581$	$1.738 \pm 0.027$	$1.567 \pm 0.206$	$0.977 \pm 0.126$	$-37.687 \pm 11.487$
IPSL-CM5A-LR	$-0.749 \pm 0.045$	$6.137 \pm 0.229$	$2.034 \pm 0.034$	$0.747 \pm 0.048$	$0.880 \pm 0.053$	$17.770 \pm 10.304$
IPSL-CM5A-MR	$-0.771 \pm 0.045$	$6.408 \pm 0.232$	$2.134 \pm 0.028$	$0.769 \pm 0.047$	$0.916 \pm 0.053$	$19.125 \pm 10.084$
IPSL-CM5B-LR	$-0.971 \pm 0.086$	$5.087 \pm 0.319$	$1.227 \pm 0.055$	$0.969 \pm 0.088$	$0.828 \pm 0.071$	$-14.597 \pm 10.716$
MIROC-ESM	$-0.753 \pm 0.046$	$7.575 \pm 0.274$	$2.852 \pm 0.034$	$0.751 \pm 0.049$	$1.013 \pm 0.062$	$34.833 \pm 12.051$
MIROC5	$-1.551 \pm 0.104$	$8.511 \pm 0.416$	$2.041 \pm 0.060$	$1.548 \pm 0.108$	$1.387 \pm 0.094$	$-10.373 \pm 8.732$
MPI-ESM-LR	$-1.081 \pm 0.073$	$7.874 \pm 0.375$	$1.997 \pm 0.051$	$1.079 \pm 0.076$	$1.260 \pm 0.085$	$16.807 \pm 11.376$
MPI-ESM-MR	$-1.101 \pm 0.078$	$7.665 \pm 0.392$	$1.864 \pm 0.058$	$1.099 \pm 0.081$	$1.244 \pm 0.088$	$13.195 \pm 11.615$
MPI-ESM-P	$-1.115 \pm 0.074$	$7.843 \pm 0.370$	$1.942 \pm 0.059$	$1.113 \pm 0.077$	$1.265 \pm 0.084$	$13.674 \pm 10.892$
MRI-ESM1	$-1.312 \pm 0.037$	$6.708 \pm 0.137$	$1.363 \pm 0.031$	$1.309 \pm 0.045$	$1.146 \pm 0.038$	$-12.441 \pm 4.169$
MRI-CGCM3	$-1.215 \pm 0.035$	$6.290 \pm 0.129$	$1.413 \pm 0.032$	$1.212 \pm 0.043$	$1.046 \pm 0.035$	$-13.736 \pm 4.204$

Similarly, the climate feedback ( $\alpha$ ) also shows a larger spread from  $-46\%$  to  $57\%$  with respect to the MMM (the fifth column in Table 2).

The MIROC-ESM model shows a  $\sim 35\%$  larger warming than that shown by the MMM (Case I), which is mainly due to the difference in climate feedback ( $\sim 25\%$  less than that in the MMM), whereas the forcing is almost the same as that in the MMM. Similarly, the INM-CM4 model shows a small difference in the forcing ( $\sim 2\%$  less than that in the MMM), whereas the feedback is  $\sim 57\%$  more than that in the MMM, leading to  $\sim 38\%$  lower ECS than that in the MMM (Case III). The CSIRO-Mk3.6.0 model shows the largest reduction in forcing and feedbacks (approximately  $-43\%$  and  $-47\%$ , respectively), but since the changes in both forcing and feedback are comparable, the net impact on ECS remains small ( $\sim 6\%$ ).

It is interesting to note that different models from the same modeling center also show different variations in ECS, climate forcing, and climate feedbacks. For instance, the MIROC5 and MIROC-ESM models are quite different when compared with the pair of MRI models (CGCM3 and ESM1). The MIROC5 model shows  $\sim 10\%$  less warming than that in the MMM, whereas the MIROC-ESM model shows  $\sim 35\%$  more warming than that in the MMM. The forcing for MIROC-ESM is close to the MMM, but the feedback is relatively smaller ( $\sim -25\%$ ), whereas, for MIROC5, the feedback and forcing are approximately  $55\%$  and  $39\%$  larger, respectively.

Similar to the intermodel comparison with respect to the MMM presented above, one can also compare the outputs of other models with respect to one benchmark model. In such a case, ctrl can be replaced with the benchmark model, and each model that is being compared can be represented by expt. It is also possible to examine the spread in ECS, climate forcing, and climate feedbacks for different ensemble members in a large ensemble of simulations conducted using a single model (e.g., Dessler et al. 2018), with the ensemble mean as ctrl and individual members as expt.

#### 4. Concluding remarks

We proposed a new graphical method that provides a concise summary of the impact of model or process change on ECS, climate forcing, and climate feedbacks. The method is based on the linear regression method that was introduced by Gregory et al. (2004). Using this method, one can (a) quantify whether the model or process change amplifies, reduces, or has no impact on global warming, (b) evaluate the percentage changes in ECS, climate forcing, and climate feed-

backs, and (c) quantify the ranges of the uncertainties in the estimated changes. Using this graph, the outputs of multiple models for the same experimental framework (e.g., usage of interactive chemistry compared with the prescribed one) can be collated and visualized in one single diagram, which is otherwise challenging to compare and comprehend.

We demonstrated this method using an example of climate sensitivity simulations with and without interactive chemistry with JMA-MRI climate models. An application of this method for four individual radiative components (CS and CRE for LW and SW components) was also described, after confirming the appropriateness of the linear fittings of Gregory's regression. We also presented the application of this method to visualize and quantify the spread in ECS, climate forcing, and climate feedbacks for individual models with respect to the MMM in multiple model frameworks such as CMIP5 (Taylor et al. 2012), Coupled Model Intercomparison Project Phase 6 (CMIP6; Eyring et al. 2016), Geoengineering Model Intercomparison Project (GeoMIP; Kravitz et al. 2011), and nonlinear climate responses to  $\text{CO}_2$  (nonlinMIP; Good et al. 2016). Furthermore, it could be used to determine the differences in these three parameters for multiple models against any benchmark model instead of the MMM or to estimate the spread or change in the three parameters for a large ensemble of simulations done by using a single model (e.g., Dessler et al. 2018).

It is also important to remark here that this method is based on Gregory's linear regression and the uncertainties (or standard errors) in climate forcing and climate feedbacks are calculated under the approximation that the relationship between the net radiative imbalance,  $\Delta N(t)$ , and the global mean surface air temperature change,  $\Delta T(t)$ , is linear. The nonlinear response of  $\Delta T$  to  $\Delta N$ , if any, will be included in the uncertainty estimates given in Subsection 2.3. In this paper, we described the graphical method and demonstrated its application using an example of climate sensitivity simulations for instantaneously quadrupled  $\text{CO}_2$  with and without interactive chemistry. More detailed findings on the impact of using interactive chemistry on the surface and other atmospheric variables in the MRI climate models will be provided in a separate paper.

#### Acknowledgments

The authors acknowledge Dr. Satoshi Noda and colleagues of the JMA MRI for providing the simulation data used in this paper. The CMIP5 data were

obtained from the ESGF website. The authors are also thankful to Professor Jonathan M. Gregory for the personal discussion provided in Subsection 2.1. This work is partially supported by JSPS KAKENHI Grant Numbers JP15H05816 and JP17H01159, JSPS Core-to-Core program B (Asia-Africa Science Platforms), JSPS & DG-RSTHE Joint Research Program, and DST Centre of Excellence in Climate Modeling. This work and its contributors (SJ and RMD) were partially supported by the UK-China Research & Innovation Partnership Fund through the Met Office Climate Science for Service Partnership (CSSP) China as part of the Newton Fund. The authors declare no financial conflict of interests.

### References

- Adachi, Y., S. Yukimoto, M. Deushi, A. Obata, H. Nakano, T. Y. Tanaka, M. Hosaka, T. Sakami, H. Yoshimura, M. Hirabara, E. Shindo, H. Tsujino, R. Mizuta, S. Yabu, T. Koshiro, T. Ose, and A. Kitoh, 2013: Basic performance of a new earth system model of the Meteorological Research Institute (MRI-ESM1). *Pap. Meteor. Geophys.*, **64**, 1–19.
- Aldrin, M., M. Holden, P. Guttorp, R. B. Skeie, G. Myhre, and T. K. Berntsen, 2012: Bayesian estimation of climate sensitivity based on a simple climate model fitted to observations of hemispheric temperatures and global ocean heat content. *Environmetrics*, **23**, 253–271.
- Andrews, T., J. M. Gregory, M. J. Webb, and K. E. Taylor, 2012: Forcing, feedbacks and climate sensitivity in CMIP5 coupled atmosphere-ocean climate models. *Geophys. Res. Lett.*, **39**, L09712, doi:10.1029/2012GL051607.
- Annan, J. D., and J. C. Hargreaves, 2006: Using multiple observationally-based constraints to estimate climate sensitivity. *Geophys. Res. Lett.*, **33**, L06704, doi:10.1029/2005GL025259.
- Bohm, G., and G. Zech, 2014: *Introduction to Statistics and Data Analysis for Physicists*. Hamburg: DESY, 469 pp.
- Chiodo, G., and L. M. Polvani, 2016: Reduction of climate sensitivity to solar forcing due to stratospheric ozone feedback. *J. Climate*, **29**, 4651–4663.
- Dessler, A. E., and P. M. Forster, 2018: An estimate of equilibrium climate sensitivity from interannual variability. *J. Geophys. Res.: Atmos.*, **123**, 8634–8645.
- Dessler, A. E., T. Mauritsen, and B. Stevens, 2018: The influence of internal variability on Earth's energy balance framework and implications for estimating climate sensitivity. *Atmos. Chem. Phys.*, **18**, 5147–5155.
- Deushi, M., and K. Shibata, 2011: Impacts of increases in greenhouse gases and ozone recovery on lower stratospheric circulation and the age of air: Chemistry-climate model simulations up to 2100. *J. Geophys. Res.*, **116**, D07107, doi:10.1029/2010JD015024.
- Dietmüller, S., M. Ponater, and R. Sausen, 2014: Interactive ozone induces a negative feedback in CO<sub>2</sub>-driven climate change simulations. *J. Geophys. Res.: Atmos.*, **119**, 1796–1805.
- Eyring, V., S. Bony, G. A. Meehl, C. A. Senior, B. Stevens, R. J. Stouffer, and K. E. Taylor, 2016: Overview of the Coupled Model Intercomparison Project phase 6 (CMIP6) experimental design and organization. *Geosci. Model Dev.*, **9**, 1937–1958.
- Good, P., T. Andrews, R. Chadwick, J.-L. Dufresne, J. M. Gregory, J. A. Lowe, N. Schaller, and H. Shiogama, 2016: NonlinMIP contribution to CMIP6: Model intercomparison project for non-linear mechanisms: Physical basis, experimental design and analysis principles (v1. 0). *Geosci. Model Dev.*, **9**, 4019–4028.
- Gregory, J. M., W. J. Ingram, M. A. Palmer, G. S. Jones, P. A. Stott, R. B. Thorpe, J. A. Lowe, T. C. Johns, and K. D. Williams, 2004: A new method for diagnosing radiative forcing and climate sensitivity. *Geophys. Res. Lett.*, **31**, L03205, doi:10.1029/2003GL018747.
- Kravitz, B., A. Robock, O. Boucher, H. Schmidt, K. E. Taylor, G. Stenchikov, and M. Schulz, 2011: The Geoengineering Model Intercomparison Project (GeoMIP). *Atmos. Sci. Lett.*, **12**, 162–167.
- Lewis, N., and J. A. Curry, 2015: The implications for climate sensitivity of AR5 forcing and heat uptake estimates. *Climate Dyn.*, **45**, 1009–1023.
- Marsh, D. R., J.-F. Lamarque, A. J. Conley, and L. M. Polvani, 2016: Stratospheric ozone chemistry feedbacks are not critical for the determination of climate sensitivity in CESM1 (WACCM). *Geophys. Res. Lett.*, **43**, 3928–3934.
- Montgomery, D. C., E. A. Peck, and G. G. Vining, 2012: *Introduction to Linear Regression Analysis*. John Wiley and Sons, 672 pp.
- Muthers, S., J. G. Anet, A. Stenke, C. Raible, E. Rozanov, S. Brönnimann, T. Peter, F. X. Arfeuille, A. I. Shapiro, J. Beer, F. Steinhilber, Y. Brugnara, and W. Schmutz, 2014: The coupled atmosphere-chemistry-ocean model SOCOL-MPIOM. *Geosci. Model Dev.*, **7**, 2157–2179.
- Naito, Y., and S. Yoden, 2005: A statistical analysis on the effects of the equatorial QBO on the extratropical stratosphere and troposphere based on large samples of daily data. *SOLA*, **1**, 17–20.
- Noda, S., K. Kodera, Y. Adachi, M. Deushi, A. Kitoh, R. Mizuta, S. Murakami, K. Yoshida, and S. Yoden, 2017: Impact of interactive chemistry of stratospheric ozone on Southern Hemisphere paleoclimate simulation. *J. Geophys. Res.: Atmos.*, **122**, 878–895.
- Noda, S., K. Kodera, Y. Adachi, M. Deushi, A. Kitoh, R. Mizuta, S. Murakami, K. Yoshida, and S. Yoden, 2018: Mitigation of global cooling by stratospheric chemistry feedbacks in a simulation of the Last Glacial Maximum. *J. Geophys. Res.: Atmos.*, **123**, 9378–9390.

- Nowack, P. J., N. L. Abraham, A. C. Maycock, P. Braesicke, J. M. Gregory, M. M. Joshi, A. Osprey, and J. A. Pyle, 2015: A large ozone-circulation feedback and its implications for global warming assessments. *Nat. Climate Change*, **5**, 41–45.
- Nowack, P. J., P. Braesicke, N. L. Abraham, and J. A. Pyle, 2017: On the role of ozone feedback in the ENSO amplitude response under global warming. *Geophys. Res. Lett.*, **44**, 3858–3866.
- Nowack, P. J., N. L. Abraham, P. Braesicke, and J. A. Pyle, 2018: The impact of stratospheric ozone feedbacks on climate sensitivity estimates. *J. Geophys. Res.: Atmos.*, **123**, 4630–4641.
- Otto, A., F. E. L. Otto, O. Boucher, J. Church, G. Hegerl, P. M. Forster, N. P. Gillett, J. Gregory, G. C. Johnson, R. Knutti, N. Lewis, U. Lohmann, J. Marotzke, G. Myhre, D. Shindell, B. Stevens, and M. R. Allen, 2013: Energy budget constraints on climate response. *Nat. Geosci.*, **6**, 415–416.
- Skeie, R. B., T. Berntsen, M. Aldrin, M. Holden, and G. Myhre, 2014: A lower and more constrained estimate of climate sensitivity using updated observations and detailed radiative forcing time series. *Earth Syst. Dyn.*, **5**, 139–175.
- Taylor, K. E., R. J. Stouffer, and G. A. Meehl, 2012: An overview of CMIP5 and the experiment design. *Bull. Amer. Meteor. Soc.*, **93**, 485–498.
- Yukimoto, S., H. Yoshimura, M. Hosaka, T. Sakami, H. Tsujino, M. Hirabara, T. Y. Tanaka, M. Deushi, A. Obata, H. Nakano, Y. Adachi, E. Shindo, S. Yabu, T. Ose, and A. Kitoh, 2011: *Meteorological Research Institute-Earth System Model Version 1 (MRI-ESM1) —Model description—*. Tech. Rep. Meteor. Res. Inst., No. 64, Meteor. Res. Inst., 92 pp. [Available at [https://www.mri-jma.go.jp/Publish/Technical/DATA/VOL\\_64/tec\\_rep\\_mri\\_64.pdf](https://www.mri-jma.go.jp/Publish/Technical/DATA/VOL_64/tec_rep_mri_64.pdf).]
- Yukimoto, S., Y. Adachi, M. Hosaka, T. Sakami, H. Yoshimura, M. Hirabara, T. Y. Tanaka, E. Shindo, H. Tsujino, M. Deushi, R. Mizuta, S. Yabu, A. Obata, H. Nakano, T. Koshiro, T. Ose, and A. Kitoh, 2012: A new global climate model of the Meteorological Research Institute: MRI-CGCM3 —Model description and basic performance—. *J. Meteor. Soc. Japan*, **90A**, 23–64.